THERMAL MODELING OF HIGH-LEVEL NUCLEAR WASTE DISPOSAL IN A SALT REPOSITORY

THERMAL HYDRAULICS

KEYWORDS: *salt, waste, thermal*

DYLAN R. HARP,* PHILIP H. STAUFFER, PHOOLENDRA K. MISHRA,† DANIEL G. LEVITT,‡ and BRUCE A. ROBINSON

Los Alamos National Laboratory, P.O. Box 1663 MS T003, Los Alamos, New Mexico

Received July 15, 2013
Accepted for Publication November 26, 2013
http://dx.doi.org/10.13182/NT13-110

Salt formations have received recent attention for geologic disposal of heat-generating, high-level nuclear waste (HLW). Existing investigations are summarized and expanded upon using analytical and numerical models to investigate simulated temperatures in the salt after emplacement of HLW. Analytical modeling suggests that temperature variations near canisters will be smooth, indicating that the system can be approximated by a coarsely discretized numerical model. Two multi-dimensional parameter studies explore canister configuration using characteristics from (a) defense HLW and (b) spent nuclear fuel (SNF) waste. Numerical modeling was conducted for a disposal concept consisting of emplacement of waste canisters on the floor of drifts and covering each with salt backfill. Results indicate that waste forms with U.S. Department of Energy (DOE) waste characteristics can be easily configured to maintain simulated temperatures far below 200°C at spacings as close as 0.3 m (∼1 ft), the minimum feasible spacing that could practically be achieved. For SNF waste packaged into canisters with heat loads of 1500 or 1000 W with canister spacing of 6 m (∼20 ft) and 3 m (∼10 ft), respectively, simulated temperatures can be maintained below 200°C; much higher maximum temperatures would result for designs with higher canister heat loads and smaller spacings. These results indicate that from a thermal loading perspective, in-drift disposal of HLW in salt deposits is feasible for DOE-managed waste as long as the maximum temperature is managed through proper selection of canister heat loads and spacings. The results will aid in the design of potential future field tests to confirm this conclusion.

Note: Some figures in this paper may be in color only in the electronic version.

I. INTRODUCTION

The disposal of radioactive wastes in domal or bedded salt formations has been studied for more than 50 years since the concept was first proposed by the U.S. National Academy of Sciences[1] due to the favorable disposal properties such as easy mining, salt creep entombing of waste with time, and low permeability (e.g., Refs. 2 through 5). Disposal of transuranic (TRU) waste in bedded salt has been implemented at the Waste Isolation Pilot Project (WIPP) in southern New Mexico since 1999 (http://www.wipp.energy.gov/fctshts/Chronology.pdf). Although TRU waste at WIPP is thermally cooler, with a lower radiological hazard than high-level nuclear waste[4] (HLW), disposal of HLW in salt in the United States has been studied extensively under the Used Fuel Disposition Campaign.[6]

According to Ref. 4, most of the HLW inventory in the United States can be categorized as defense high-level waste (DHLW), or used nuclear fuel (UNF) or spent nuclear fuel (SNF) from nuclear power plants. DHLW is generated from the reprocessing of some 170 000 tonnes heavy metal from nuclear fuel used for defense purposes as

*E-mail: dharp@lanl.gov
†Currently with California State University, Fullerton
‡Currently with Neptune and Company, Inc.

well as U.S. Department of Energy (DOE)-owned SNF, which includes fuel from reactors used for research and defense purposes, fuel from the U.S. Naval propulsion program (naval fuel), and some recovered damaged fuel from Three Mile Island. In contrast to civilian UNF, SNF is used to describe DOE-managed fuels because it is very unlikely that it would ever be reprocessed even if recycling is adopted for civilian UNF. DHLW in the form of borosilicate glass waste forms at the Savannah River Site (SRS) is awaiting disposal in a HLW repository. Large quantities of HLW are also present in various forms at SRS, the Hanford Site, and Idaho National Laboratory. HLW resulting from reprocessing activities at West Valley, New York, is also awaiting disposal. Reference 4 points out that there is no known technical issue related to safety or adverse environmental impact that creates an urgent need to identify a permanent disposal option for civilian UNF. One of the strategies under consideration is to locate UNF from roughly 70 current and former nuclear power plant sites in one or more storage facilities. In contrast, DHLW has no conceivable future value and should be permanently disposed of in a geologic repository as soon as one is available.

The objective of this study is to investigate the thermal regime created by disposal of defense wastes in a salt repository. The wastes have a variety of thermal loads, including modest heat loads from existing and projected vitrified waste canisters of DHLW, as well as higher thermal load waste forms (e.g., SNF waste canisters with initial heat loads ≥ 1000 W). For simplicity, we refer to the relatively lower thermal load waste canisters as DHLW and the relatively higher thermal load canisters as SNF.

Generally speaking, salt is presumed to have the advantage of supporting higher maximum temperatures in the rock mass than other disposal media such as clay and granite (e.g., Ref. 6). Throughout this paper, we use a target temperature of 200°C as the proposed maximum temperature induced by the disposal of HLW to limit uncertainty in performance assessment. This value is commonly used (e.g., Ref. 7), even though higher peak temperatures may be possible if supported by test data.[6]

Simulations of heat flow in salt were conducted using the Los Alamos National Laboratory porous flow simulator known as the finite element heat and mass transfer code (FEHM) (http://fehm.lanl.gov/, Ref. 8). The model considers purely diffusive energy transport. Materials are approximated using bulk thermal properties, and heat conductivity is temperature dependent. The heat sources are constant over time and taken as the initial heat load of the canisters. The model considers the following materials: canister, run-of-mine salt, air gap, and intact salt. Both steady-state and transient temperature profiles have been studied. FEHM has been used extensively for simulations involving multiphase heat and mass transport and has been cited in over 100 peer-reviewed publications.[9] The present simulations investigate the temperature regimes generated by the disposal of DHLW canisters in a generic salt repository. These simulations build on the lessons learned from previous heat flow simulations in bedded salt formations, including those described in Ref. 10, which describe three-dimensional (3-D) simulations that were conducted using FEHM to simulate heat flow in a generic salt repository. Effects on the temperature regime due to moisture movement, mechanical deformation, chemical precipitation and dissolution, and heat load decay are not considered here but are currently being investigated and will be presented in future publications.

Heat flow simulations performed for this paper are conducted using both multidimensional parameter studies and a Monte Carlo sampling approach to investigate various waste canister disposal configurations. Two multidimensional parameter studies are conducted, one for thermal loads consistent with DHLW and the other focused on SNF heat loads. The Monte Carlo analysis investigates uncertainty in temperatures due to variable heat loads in the DOE waste inventory. These analyses are intended to answer the following types of questions:

1. What maximum canister-salt contact temperature is likely to be reached?
2. How far vertically and laterally from waste canisters do elevated temperatures reach?
3. How does canister burial depth in run-of-mine salt impact temperature profiles?
4. How does canister spacing impact temperature profiles?

II. METHODOLOGY

II.A. Material Properties

Reference 11 investigates the temperature dependence of the thermal conductivity K ($\mathrm{W \cdot m^{-1} \cdot K^{-1}}$) of intact salt at the WIPP, identifying the following relationship:

$$K_{T-\mathrm{WIPP}}(T) = K_{T-300}\left(\frac{300}{T}\right)^{1.14} , \tag{1}$$

where K_{T-300} is the thermal conductivity at 300 K ($5.4\ \mathrm{W \cdot m^{-1} \cdot K^{-1}}$) and T is the temperature in kelvin (K); this relationship is used for the thermal conductivity of intact salt in this paper.

Reference 12 investigates the dependence of thermal conductivity on the porosity ϕ of run-of-mine salt at the Asse salt mine in Germany. The authors developed the following relationship fitting the thermal conductivity of run-of-mine salt to porosity (ϕ) using a fourth-order polynomial as

$$K_{T-ASSE}(\phi) = -270\phi^4 + 370\phi^3 - 136\phi^2 + 1.5\phi + 5 \ . \quad (2)$$

To combine the findings of Refs. 11 and 12, K_{T-ASSE} has been scaled to match K_{T-300} at $\phi = 0$ as

$$K_{T-300}(\phi) = \left(\frac{K_{T-300}}{K_{T-ASSE}(\phi=0)}\right) K_{T-ASSE}(\phi) \ , \quad (3)$$

where K_{T-300}/K_{T-ASSE} ($\phi = 0$) is 5.4/5.0 or 1.08. Equations (1) and (2) were derived using data from domal and bedded salt formations, respectively. The relationship of thermal conductivity to temperature and porosity may not be the same in these formations. The combination of Eqs. (1) and (2) allows the available information on salt thermal properties to be incorporated in this generic salt repository study, while further experimental investigations are still needed. Following Ref. 10, the assumption has been made here that run-of-mine salt has the same temperature dependence as intact salt, giving

$$K_{T-crushed}(T, \phi) = K_{T-300}(\phi)\left(\frac{300}{T}\right)^{1.14} \ . \quad (4)$$

These material properties of salt and the other material properties used in this paper are presented in Table I and are consistent with values available in the literature.[10] The temperature dependence of the specific heat capacity is not considered here.

II.B. Analytical and Numerical Model Comparison

Heat diffusion in intact salt due to a heated HLW cylinder of infinite length is investigated here using a radial analytical model and a two-dimensional (2-D) radial numerical FEHM model. The results from the two models are compared for two purposes: (a) to verify the proper setup of the FEHM model runs and (b) to examine the temperature profiles near the canister-salt interface at a resolution greater than can be practically achieved in a large-scale simulation. High-resolution simulations of temperature variations between canisters performed using the analytical model are presented.

II.B.1. Analytical Model of a Heated Cylinder

We implement a two-material heat flow solution with constant thermal conductivities as given by Ref. 13. Although the problem of interest has temperature-dependent thermal properties, the use of constant properties is warranted for the purposes of model verification and examination of fine-scale details near the canister-salt interface. A cylinder of infinite length is approximated in a radial model as a heated 2-D disk. Consider a region with cylindrical coordinates where $0 \le r < a$ is one material (waste) with thermal conductivity K_1, specific heat capacity $C_{p,1}$, and density ρ_1 and another region where $r > a$ is another material (salt) with properties K_2, $C_{p,2}$, and ρ_2. Consider both materials to be at zero temperature initially and that there is a source producing heat at a constant rate q_0 per unit time per unit volume in region $0 \le r < a$ for all time ($t > 0$). The heat flow in these materials under such conditions is governed by

$$K_1\left\{\frac{\partial^2 T_1}{\partial r^2} + \frac{1}{r}\frac{\partial T_1}{\partial r}\right\} - C_{p,1}\rho_1\left(\frac{\partial T_1}{\partial t}\right) = -q_0 \quad (5)$$

and

$$K_2\left\{\frac{\partial^2 T_2}{\partial r^2} + \frac{1}{r}\frac{\partial T_2}{\partial r}\right\} - C_{p,2}\rho_2\left(\frac{\partial T_2}{\partial t}\right) = 0 \ . \quad (6)$$

TABLE I

Material Properties

Material	Thermal Conductivity, K ($W \cdot m^{-1} \cdot K^{-1}$)	Specific Heat Capacity ($J \cdot kg^{-1} \cdot K^{-1}$)	Density, ρ (kg/m^3)	Porosity, ϕ	Thermal Diffusivity, k [$m^2/s = K/(\rho C_p)$]
Waste	1.0	840	2220	0.001	5.40E−07[a]
Intact salt	Eq. (1), 5.3 at 30°C Eq. (1), 3.2 at 200°C	931	2190	0.01	2.6E−6 at 30°C 1.6E−6 at 200°C
Run-of-mine salt	Eq. (4), 0.72 at 30°C Eq. (4), 0.43 at 200°C	931	1423	0.35	5.5E−7 at 30°C 3.3E−7 at 200°C
Air	0.03	1000	1.0	0.999	3.00E−05

[a]Read as 5.40×10^{-7}.

Using the Laplace transform, Ref. 13 has a solution to these equations:

$$T_1(r) = \frac{4q_0 K_2 \kappa_2}{\pi^2 a} \int_0^\infty \frac{\left(1 - e^{-\kappa_1 u^2 t}\right) J_0(ur)\, J_1(ua)}{u^4 \left[\chi^2(u) + \psi^2(u)\right]} du \; , \tag{7}$$

and

$$T_2(r) = \frac{2q_0 \sqrt{\kappa_2}}{\pi} \int_0^\infty \frac{\left(1 - e^{-\kappa_1 u^2 t}\right) J_1(ua)[J_0(\kappa ur)\chi(u) - Y_0(\kappa ur)\psi(u)]}{u^3 \left[\chi^2(u) + \psi^2(u)\right]} du \; , \tag{8}$$

where T_1 is valid for $0 \leq r < a$; T_2 is valid for $r > a$; $\kappa_1 = K_1/(\rho_1 C_{p,1})$ and $\kappa_2 = K_2/(\rho_2 C_{p,2})$ are the thermal diffusivities of materials 1 and 2, respectively; $\kappa = \sqrt{\kappa_1/\kappa_2}$; J_0 and J_1 are zeroth- and first-order Bessel functions, respectively, of the first kind; and Y_0 is a zeroth-order Bessel function of the second kind. The function χ is defined as

$$\chi(u) = K_1 \kappa_2^{0.5} J_1(au) Y_0(\kappa au) - K_2 \kappa_1^{0.5} J_0(au) Y_1(\kappa au) \tag{9}$$

while ψ is defined as

$$\psi(u) = K_1 \kappa_2^{0.5} J_1(au) J_0(\kappa au) - K_2 \kappa_1^{0.5} J_0(au) J_1(\kappa au) \; , \tag{10}$$

where Y_1 is a first-order Bessel function of the second kind.

II.B.2. Numerical Model of a Heated Cylinder

Heat diffusion in salt due to a heated cylinder is modeled with a 2-D radial (r-z) FEHM model with unit depth (1 m) in the z-direction (Fig. 1). Nodes in the radial (r) direction are evenly spaced at 3.048×10^{-3} m (10^{-2} ft) from $0 \leq r \leq 0.3048$ m (1 ft) and increasing logarithmically from 0.3048 to 1000 m. Nodes for $0 \leq r \leq 0.3048$ m comprise the heated cylinder (waste canister) while the remainder of the nodes are salt. The top and bottom boundaries ($z = 0$ and $z = 1$ m) are reflection (no flow) boundaries. Therefore, similar to the analytical model, this model approximates a cylinder of infinite length. The numerical model is solved for both constant and temperature-dependent thermal conductivity of intact salt [refer to Eq. (1) for the temperature-dependent relation].

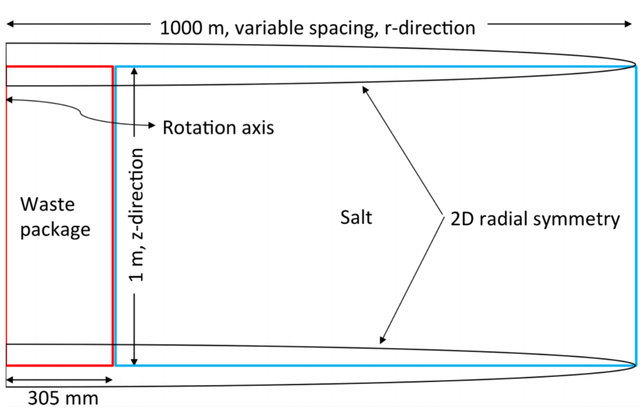

Fig. 1. Schematic diagram of 2-D radial numerical model.

II.B.3. Comparison of Analytical and Numerical Models

Figure 2a compares temperatures simulated by both models using intact-salt properties with constant thermal conductivities of 5.0 $W \cdot m^{-1} \cdot K^{-1}$ at various radial distances from the center of the cylinder. This plot demonstrates that the numerical model captures the behavior of the analytical model. For Fig. 2b, the temperature-dependent thermal conductivity algorithms implemented in FEHM are used and are bounded by analytically simulated temperatures using constant thermal conductivities calculated at the upper (68°C) and lower (30°C) temperature limits from the FEHM model. The temperatures simulated analytically with constant thermal conductivities bound the FEHM run, indicating that the temperature-dependent thermal conductivity relation implemented in FEHM is reasonable.

II.B.4. Waste-Salt Interface

For the 3-D numerical model simulations described below, the material contact cannot be captured at high resolution. In fact, we have node spacing of the order of 0.3 m (1 ft) around the waste canisters so that each waste canister is 2 nodes wide $\times$ 2 nodes high $\times$ 3 nodes long (nodes are 0.5 m in the length direction, and only half of the canisters are modeled explicitly). The analytical approach allows us to explore the temperature variation at a much higher resolution. The analytical model is used to investigate the temperature between two 500-W waste canisters of infinite length embedded in run-of-mine salt at 1000 years after emplacement. The principle of superposition is used to combine the thermal effects of the canisters with 0.3048 m (1 ft) between their surfaces [0.9144 m (3 ft) between canister centers]. Figure 3 presents the simulated temperatures between canisters, where it is apparent that the simulated temperatures near

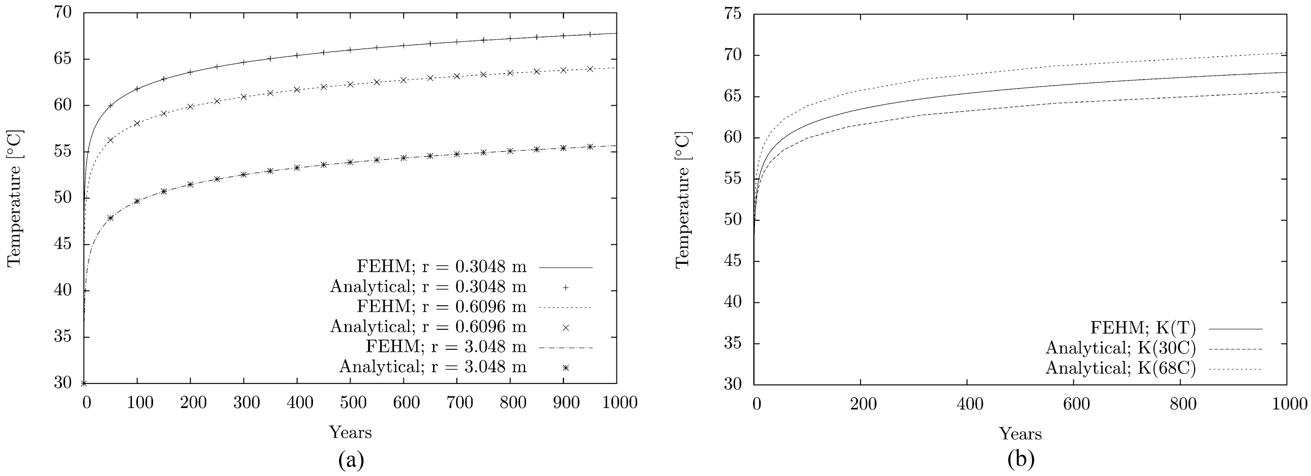

Fig. 2. Comparison of analytical and numerical models of heat conduction from heated disks embedded in intact salt. (a) Temperatures simulated by both models using intact-salt properties with constant thermal conductivities of 5.0 $W \cdot m^{-1} \cdot K^{-1}$ at various radial distances from the center of the disk are compared. (b) Temperatures from the temperature-dependent thermal conductivity algorithms implemented in FEHM are bounded by analytically simulated temperatures using constant thermal conductivities calculated at the upper and lower temperature limits from the FEHM model.

the waste-salt interface are smooth. This indicates that a coarse numerical mesh will provide a reasonable approximation of temperature variations.

II.C. Thermal Loads of Waste Canisters

Table II shows an estimate of waste container heat loads for all DOE HLW that may be available by the year 2023 (Ref. 14). These data show that 98.9% of the expected waste canisters have heat loads $\leq$220 W. These data are used to guide parameter study 1. Table II is also used to populate the distribution of canister heat loads in the Monte Carlo analysis. SNF waste forms are simulated as naval fuel waste forms, which consist of 400 canisters, 45 000 kg (98 000 pounds) each, totaling 1.7 MW. The SNF simulations are predicated on the assumption that these large canisters, each over 2000 W, will be repackaged into a greater number of smaller canisters with lower heat loads of between 1000 and 2000 W. Also, the total number of canisters in the SNF inventory that are $\geq$1000 W is small ($>$1% or 31/3542). Thus, by examining high (2000 W), medium (1500 W), and low (1000 W) deterministic scenarios where each canister in a room is given the same heat load, we ensure that our simulations span the range of behavior likely to be seen in rooms packed with the hotter SNF/naval fuel components of the waste stream.

II.D. Three-Dimensional Numerical Model

II.D.1. Waste Emplacement Concept

The operational steps required to dispose of waste packages underground is called the waste emplacement

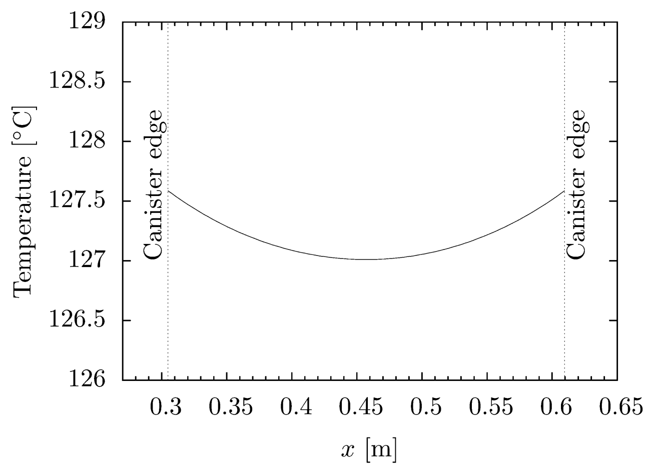

Fig. 3. Analytical calculation of temperature between two 500-W canisters of infinite length spaced 305 mm (1 ft) apart embedded in intact salt with constant thermal conductivity. The temperature profile is after 1000 years of heating. x is the distance from the center of one canister to the center of the other canister.

concept. In this study, the in-drift disposal concept described in Ref. 4 is used for the heat transfer calculations. For the in-drift concept, the waste canisters are placed on the floor along the length of a drift, one at a time, and covered with salt backfill (i.e. run-of-mine salt created during excavation of drifts) for shielding. This efficient in-drift emplacement configuration will maximize the utilization of the valuable repository space, eliminating wasted or empty space. Reference 4 discusses the operational advantages provided by the concept. At the

TABLE II

Number and Cumulative Percentage of Waste Canisters Within Heat Load Ranges for all DOE HLW Inventory*

Decay Heat per Canister (W)	Number of Canisters	Cumulative Percentage
<50	16 630	72.20%
50 to 100	1 696	79.60%
100 to 220	4 414	98.70%
220 to 300	28	98.90%
300 to 500	264	100.00%

[a]From Ref. 14, Table 3-3.

repository scale, a series of panels, each of which is a subsurface cell consisting of individual drifts, is constructed underground. Figure 4 depicts a portion of a repository suitable for conducting heat transfer analyses.

II.D.2. Model Setup

A 3-D finite-volume heat transfer model has been constructed using the computer code FEHM to investigate the temperatures due to HLW disposal in a generic salt repository. The simulations are depth independent, up to an additive constant T_0 due to the geothermal gradient and associated boundary conditions, as FEHM is only solving the heat equation here. The model domain is designed to simulate temperature evolution in a single interior "room" (i.e., drift) within a panel of rooms surrounded by other panels. Because of the symmetry of the room and surrounding panels, the model extends from the center of the room ($x = 0$ m) to the center of the salt pillar separating the room from the next room ($x = 18$ m) in the x-direction, from the centers of the access drifts located at either end of the room in the y-direction ($y = -92.65$ m to $y = 92.65$ m), and from 50 m below the room floor to 50 m above the room floor in the z-direction ($z = -50$ m to $z = 50$ m). The room itself extends from $y = -90$ m to $y = 90$ m (180 m long; ~590 ft). Figure 4 shows a schematic diagram (plan view) of the model layout with the symmetry domain highlighted by a rectangle. Figure 5 shows a 3-D representation of the model domain and a close-up of the model domain near the alcove entrance where the tapered backfill (run-of-mine) salt is apparent. The porosity and density of run-of-mine salt are assumed constant even though they will change in reality. The bury depth of run-of-mine salt in parameter study 1, which is discussed below, refers to the total depth not considering the tapered ends of the pile. The model uses an orthogonal grid with refinement within and near the room. Node spacing in the x-direction is 0.5 m along the room and expands logarithmically to the center of the pillar. Node spacing in the y-direction is 0.5 m along the access drifts and 0.3 m along the room. To capture details in the adit walls, node spacing in the z-direction is 0.3 m from 1.65 m below the room floor ($z = -1.65$ m) to 6.15 m above the floor ($z = 6.15$ m). The mesh expands logarithmically from this region of refinement to the boundaries in both the negative and positive z-directions. Figure 6 shows the orthogonal grid near the room entrance, with the refined region of the mesh near the room and the logarithmically expanding portions of the mesh. Grid generation is automated to facilitate modifications to the canister dimensions and spacing, room dimensions, and general spacing using GRIDDER (Ref. 15). To approximate the 0.6-m (~2-ft) diameter waste canisters on an orthogonal grid, the canisters are simulated as 0.6-m (~2-ft) square rectangular boxes, 3.5 m (~12 ft) long. Heat loads are distributed evenly throughout the box-shaped canisters even though their volume is approximately 1.3 times the volume of the actual canisters. The canisters are placed crosswise in the 3-m (~10-ft) high × 6.6-m (~21.5-ft) wide room.

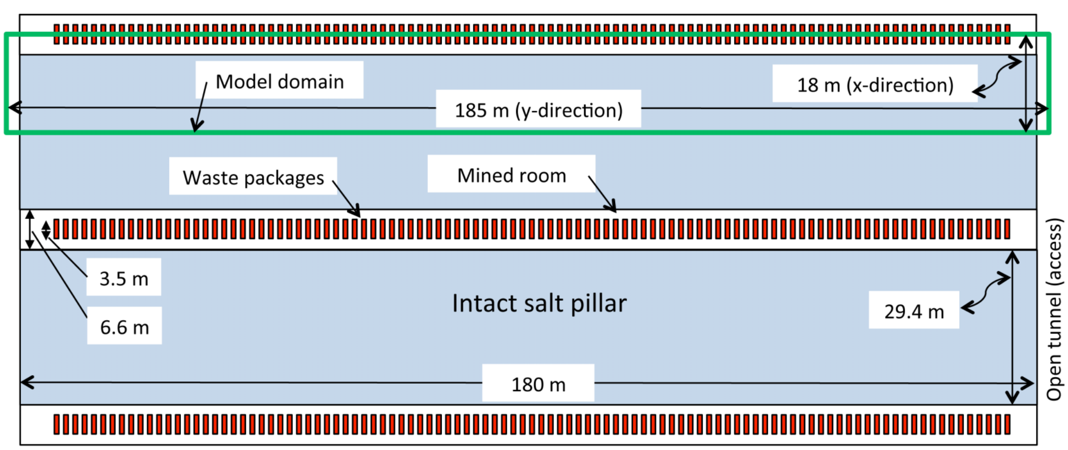

Fig. 4. Plan view of repository layout for the in-drift waste emplacement concept. The numerical model domain is outlined by a rectangle.

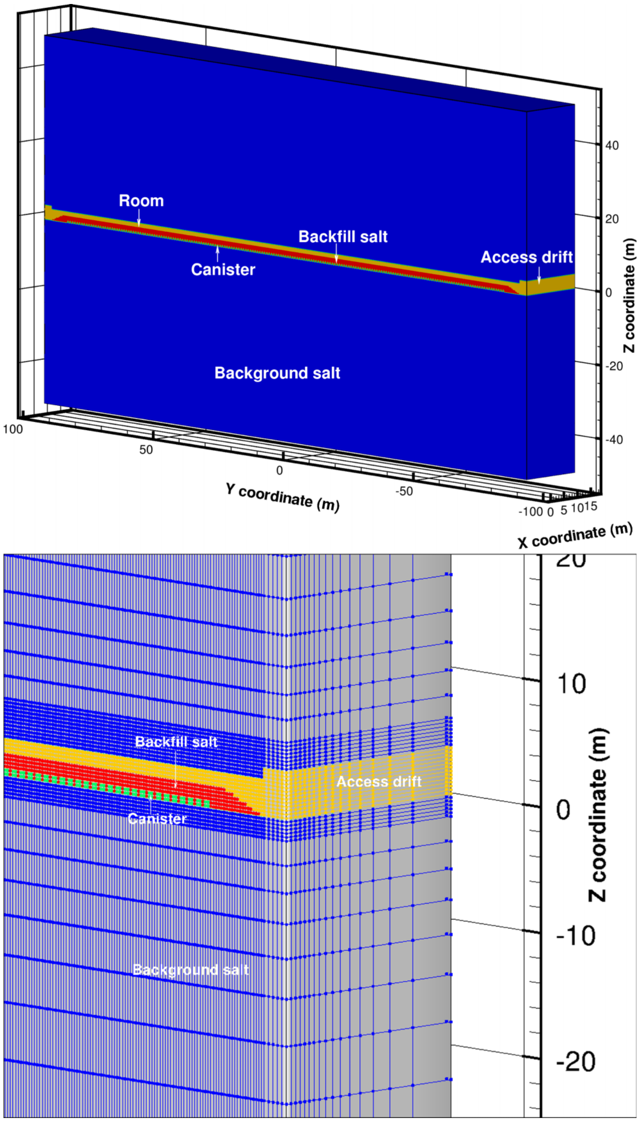

Fig. 5. Three-dimensional view of model layout specifying model materials (top), and close-up of model layout near the entrance of the alcove (bottom). The model nodes and mesh are colored according to material. The run-of-mine salt is constant over the canisters and tapers off toward the end of the alcove. The access drift and the space in the room above the backfill salt are modeled as air.

Temperature influences from the missing (i.e., not explicitly simulated) half of the room and adjacent rooms and panels are simulated using thermal reflection boundaries (no flow) along all four vertical sides of the model domain. Reflection boundaries at the centers of the access drifts at both ends of the room simulate effects from adjacent panels of rooms. Boundary conditions on the top and bottom of the model are set to fixed far-field temperatures considering a geothermal gradient so that an initial (i.e., before waste emplacement) temperature of 30°C is simulated within the room. In the simulations

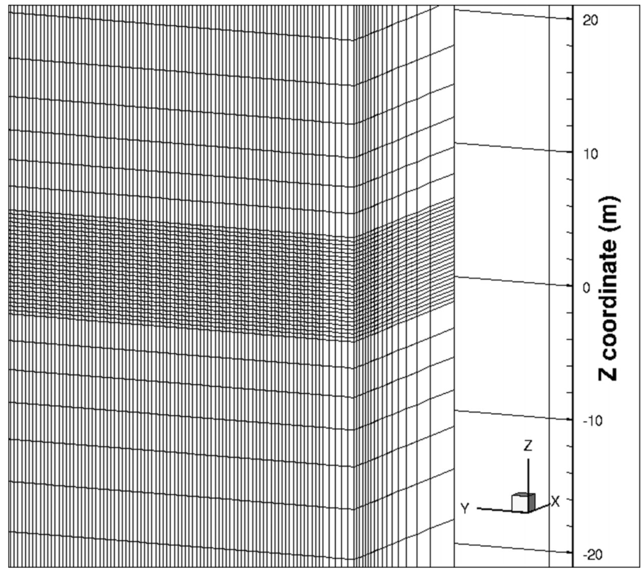

Fig. 6. Three-dimensional close-up of orthogonal grid spacing near the alcove entrance.

conducted here, heat effects did not reach the far-field boundaries. Finally, the heat loads in the waste canisters are assumed constant with no decay, leading to long-term steady-state temperature profiles as the energy flux from the canisters comes into equilibrium with the thermal gradient carrying heat to the top and bottom boundaries of the model domain. Thus, our calculations of maximum temperature are conservative (high), as the heat output of actual waste canisters will decrease through time as the heat-generating radioactive components decay.

II.D.3. Model Strategy

The Dakota toolkit[16] is used to facilitate the numerical investigations. Model simulations driven by Dakota are preprocessed using a Python script so that model factors affecting basic FEHM numerical model setup, such as canister spacing and bury depth, can be investigated in an automated fashion.

Three sets of heat flow simulations are presented—two multidimensional parameter studies and one Monte Carlo analysis:

1. Parameter Study 1
   a. DOE waste canisters
   b. bury depths of run-of-mine salt: 1.2, 1.8, 2.4, and 3.0 m (∼4, 6, 8, and 10 ft)
   c. canister heat loads: 55, 110, or 220 W
   d. canister spacing between centers: 0.9, 1.2, and 1.8 m (∼3, 4, and 6 ft)

2. Parameter Study 2

   a. SNF/naval fuel waste canisters

   b. canister heat loads: 1000, 1500, and 2000 W

   c. canister spacing between centers: 3.0 and 6.0 m (~10 and 20 ft)

   d. depth of run-of-mine salt constant at 1.8 m (6 ft)

3. Monte Carlo sampling of DOE waste loads (Table II) with a constant canister spacing of 0.9 m between centers with a 1.8-m depth of run-of-mine salt. These simulations are used to estimate probabilities associated with temperature profiles due to uncertainty in the combination of heat loads of the canisters in a room.

III. RESULTS

For all cases, transient thermal conduction is simulated, with thermal properties described in Sec. II.A. More complex models are possible in which, for example, thermal conduction is coupled to a two-phase-flow model with air, water, and water vapor to capture the impact of the small quantities of water present in the salt. Convective and latent heat effects would tend to enhance heat transfer away from the canister heat source. If these effects turn out to be important, simulated temperatures reported in the present study would err on the high side, which is advantageous when comparing these model results to a prescribed maximum temperature (200°C in this study). Models including these effects will be the subject of future studies.

III.A. General Numerical Model Behavior

Some details of general model behavior common to all the 3-D numerical simulations are described here. Figure 7 shows the time evolution of temperature for two heat loads at both the canister center and at the center of the pillar separating rooms. Based on Fig. 7, the characteristic time to a steady state is of the order of 60 years. Given that radioactive decay is neglected here, simulated steady-state temperatures provide conservative (high) estimates of temperatures. Figure 8 is a 3-D view showing the general trend of spatial temperature variation in the steady state (200 years) for a 220-W canister with 0.3-m (~1-ft) separation between canisters.

III.B. DHLW Simulations (Parameter Study 1)

The results of parameter study 1 are presented in Figs. 9, 10, and 11, where steady-state temperature profiles in the lateral (x) and vertical (z) directions for the bury depths (Fig. 9), canister heat load (Fig. 10), and

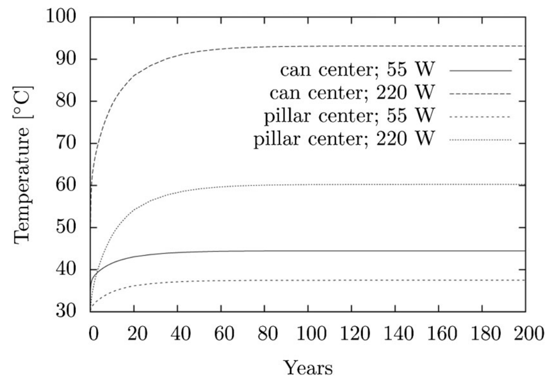

Fig. 7. Simulated temperature histories for two heat loads at two locations: "can center" [at canister center in alcove along reflection boundary ($x = 0$ m, $y = -0.15$ m, $z = 0.15$ m)] and "pillar center" [at center of pillar separating one alcove from another ($x = 18$ m, $y = -0.15$ m, $z = 0.15$ m)].

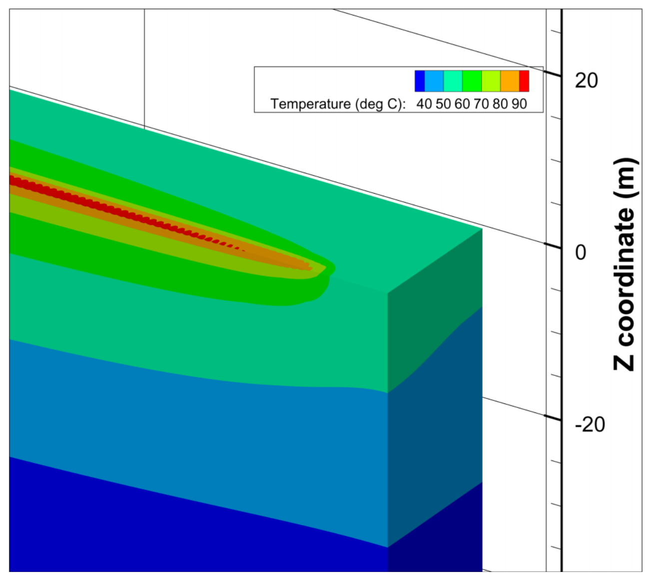

Fig. 8. Simulated temperature after 200 years with 220 W canisters. Upper part of the model is cut away to show the center of the canisters.

canister spacing (Fig. 11) are presented. Because of the differences in the thermal conductivity and diffusivity of run-of-mine salt and air (salt has higher conductivity while air has higher diffusivity; Table I and Fig. 12), interesting behavior is observed in Fig. 9: Temperatures within and near the canister increase as bury depth increases. This behavior is a result of the thermal diffusivity of run-of-mine salt being less than for air. Therefore, increased bury depths restrict the diffusion of heat away from the canisters. However, it is also apparent that as the bury depth increases, the temperature profiles cross near the room ceiling, with temperatures decreasing with increasing bury depth. This demonstrates that bury

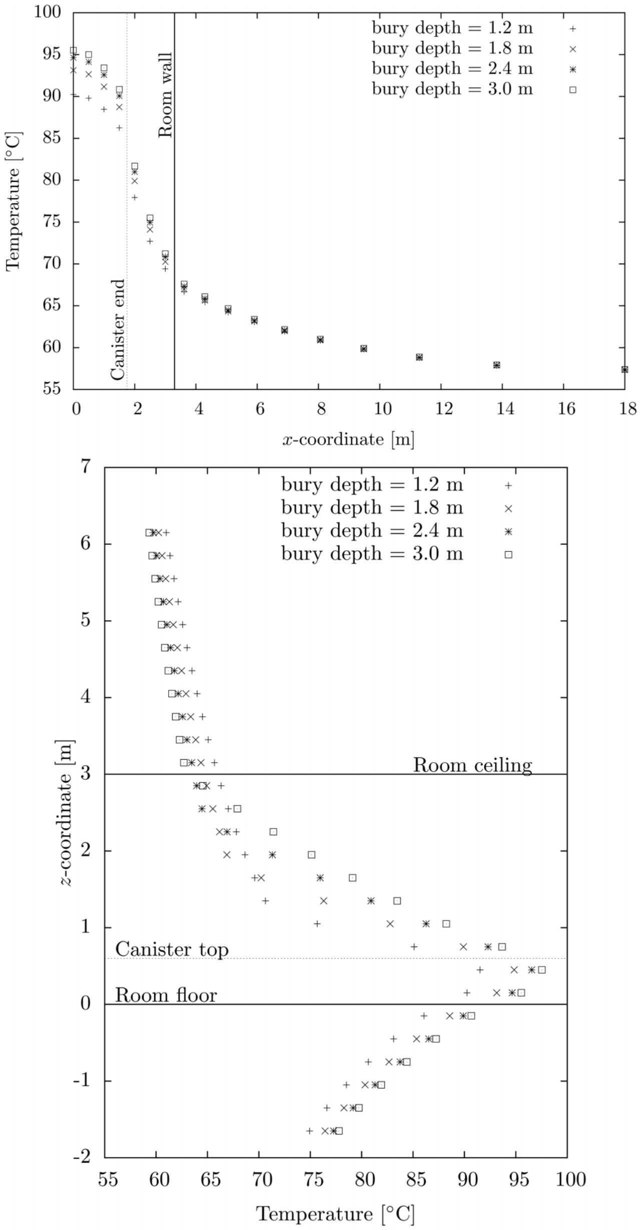

Fig. 9. Simulated steady-state temperatures at finite-volume nodes for various depths of run-of-mine salt measured from the floor of the room with 220-W canisters with centers 0.9 m apart. Upper plot presents temperature profiles in the x-direction along the line $y = -0.15$ m and $z = 0.15$ m from the center of the room through the center canister to the center of the pillar. Lower plot is in the z-direction along the line $x = 0$ m and $y = -0.15$ m from below the room through the center canister and into the ceiling.

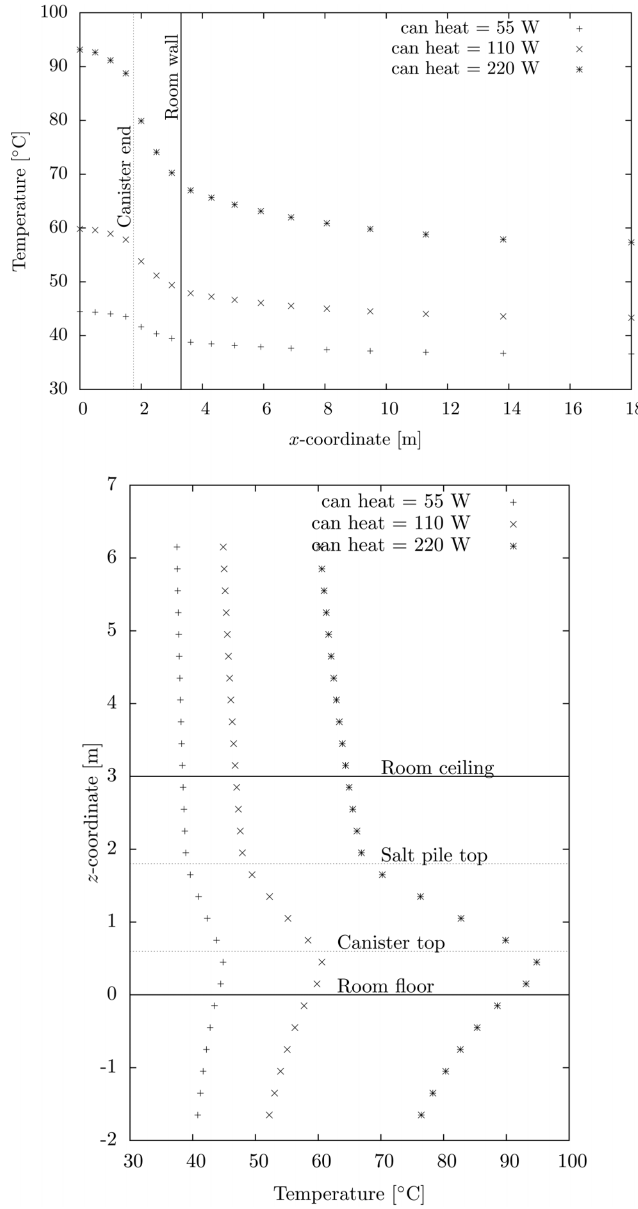

Fig. 10. Simulated steady-state temperatures at finite-volume nodes for various heat loads with centers spaced 0.9 m apart with a 1.8-m depth of run-of-mine salt measured from the floor of the room. Upper plot presents temperature profiles in the x-direction along the line $y = -0.15$ m and $z = 0.15$ m from the center of the room through a canister (can) to the center of the pillar. Lower plot is in the z-direction along the line $x = 0$ m and $y = -0.15$ m from below the room through the center canister and into the ceiling.

depth may have complicating effects on the temperature regime within a repository, such that increasing bury depth for radioactive shielding may also increase temperatures near the canisters. Exploring this behavior experimentally would be necessary to confirm this behavior.

The greatest change in temperature within a canister for various bury depths diminishes quickly with horizontal distance from the canister. Based on the sampled bury depths, the rate of temperature increase at the canister per unit bury depth decreases from 4.8°C/m to

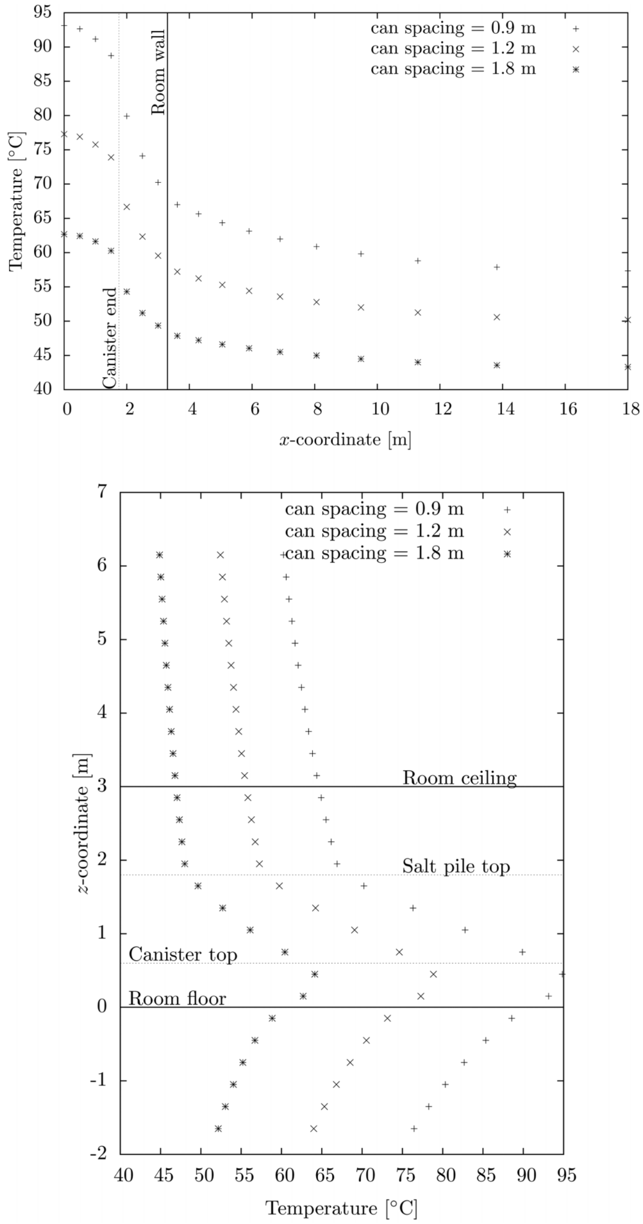

Fig. 11. Simulated steady-state temperatures at finite-volume nodes for various distances between canister centers (canister spacing) with 220-W canisters with a 1.8-m depth of run-of-mine salt measured from the floor of the room. Upper plot presents temperature profiles in the x-direction along the line $y = -0.15$ m and $z = 0.15$ m from the center of the room through a canister to the center of the pillar. Lower plot is in the z-direction along the line $x = 0$ m and $y = -0.15$ m from below the room through the center canister and into the ceiling.

1.5°C/m, indicating that the effect of increased bury depth on the canister decreases as the bury depth increases. The location of the largest rate is above the canister at $z = 1.2$ m, decreasing from 11.8°C/m to 3.3°C/m.

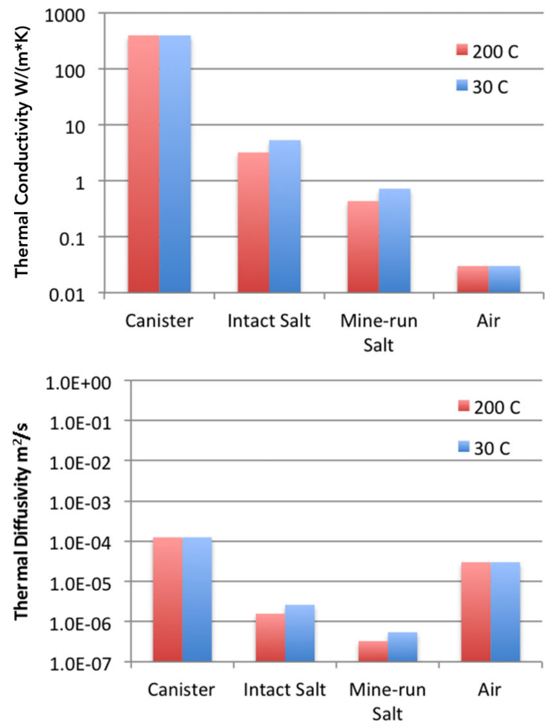

Fig. 12. Thermal conductivities and diffusivities of various materials used in the models.

In Fig. 10, the rate of temperature increase per unit canister heat is ~0.3°C/W. This rate is approximately constant (the relationship is linear) over the sampled canister heats, as expected, as canister heat is a multiplier in the diffusion equation solution.

In Fig. 11, the rate of temperature decrease per unit increase in canister spacing is from 52°C/m to 24°C/m, indicating a decrease in rate of a factor of approximately 2. This indicates that as canister spacing increases, the incremental effect on temperatures will decrease due to the increasing diffusive volume available as canister spacing increases.

III.C. SNF Simulations (Parameter Study 2)

This set of simulations is designed to show how canister spacing impacts temperature profiles for cases with 1000-, 1500-, or 2000-W canisters. Figures 13 and 14 show that the increase in temperature with canister heat is approximately linear, similar to Fig. 10. The rate of decrease in temperature decreases with increasing canister spacing, similar to Fig. 11.

Figures 13 and 14 indicate that to maintain salt temperatures below the prescribed design maximum of 200°C, repackaging to 1500- or 1000-W canisters with a canister spacing of 6 and 3 m, respectively, may be necessary. If the last 6 m of space in the rooms has no canisters, then 29 and 57 canisters can be disposed in each room with 6- and 3-m spacings, respectively.

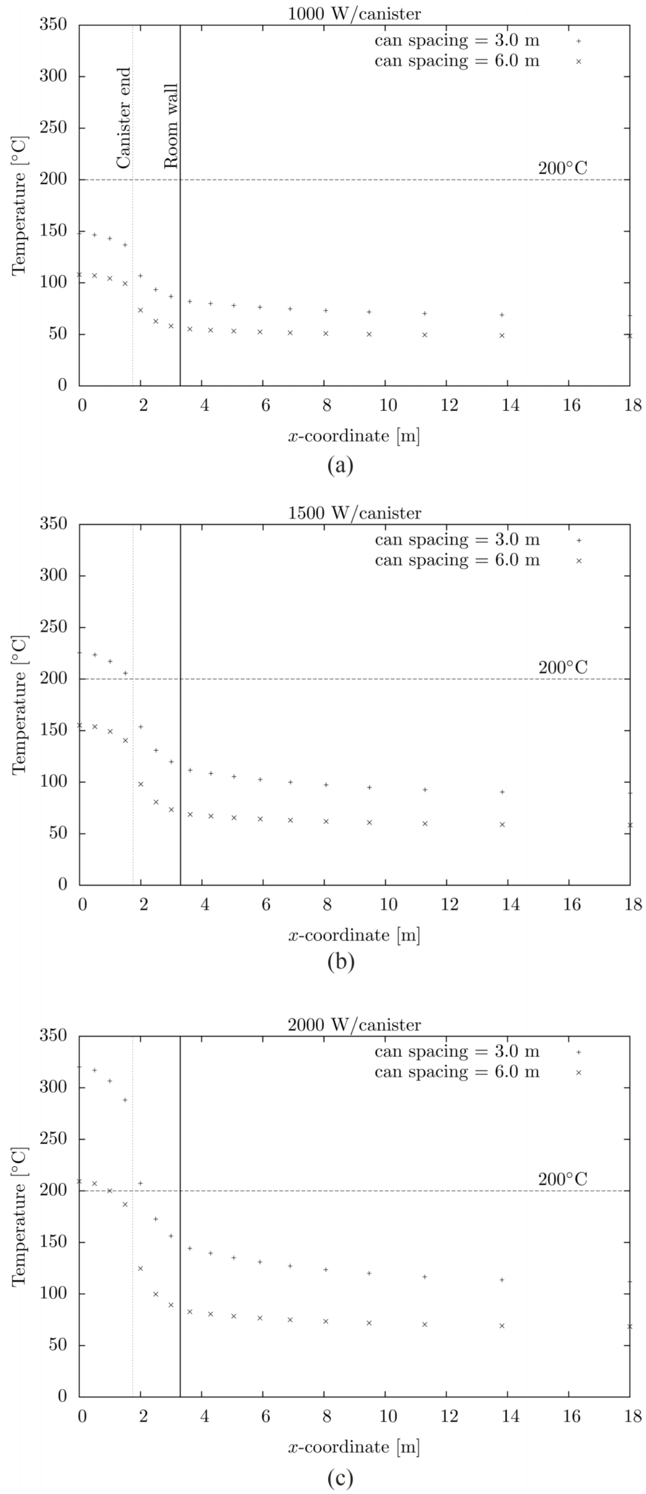

Fig. 13. Simulated steady-state temperatures at finite-volume nodes for various distances between canister centers (canister spacing) buried with 1.8 m of run-of-mine salt measured from the room floor with (a) 1000-, (b) 1500-, and (c) 2000-W canisters. Temperature profiles are in the x-direction along the line $y = -0.15$ m and $z = 0.15$ m from the center of the room through the center canister to the center of the pillar. A horizontal dashed line indicates 200°C in each plot. Temperatures far in excess of 200°C would never be considered in an actual design but are included here to illustrate the sensitivity of maximum temperature to the combination of spacing and thermal load.

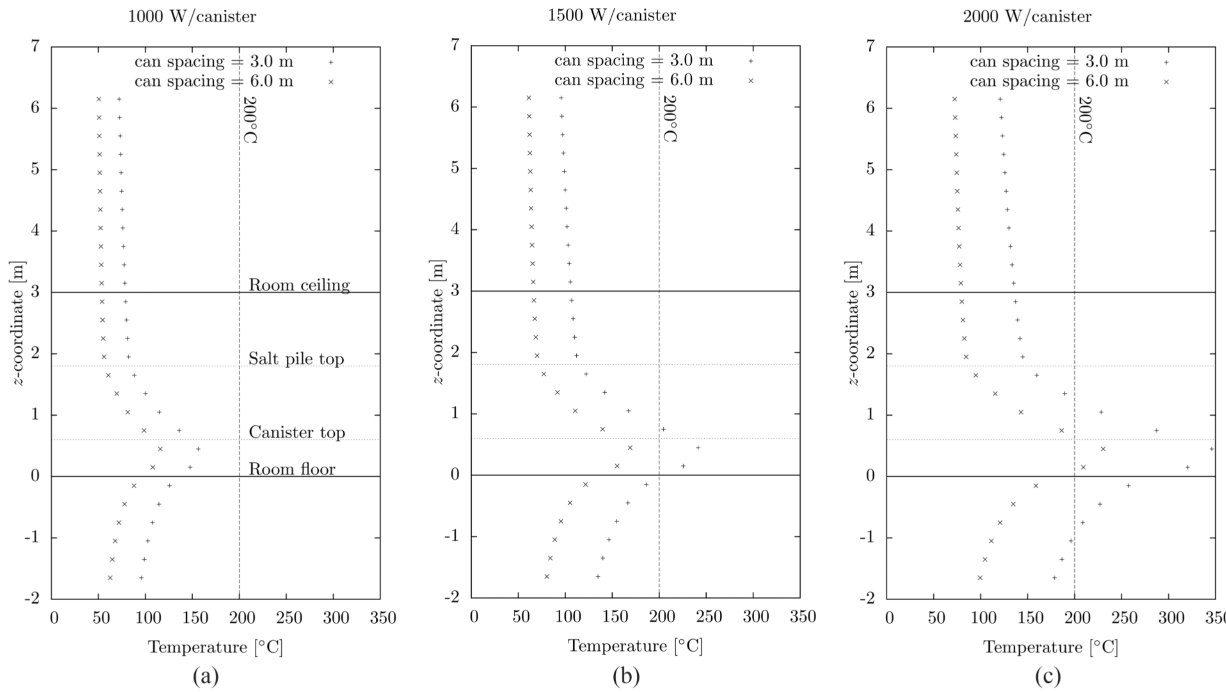

Fig. 14. Simulated steady-state temperatures at finite-volume nodes for various distances between canister centers (canister spacing) buried with 1.8 m of run-of-mine salt measured from the alcove floor with (a) 1000-, (b) 1500-, and (c) 2000-W canisters. Temperature profiles are in the z-direction along the line $x = 0$ m and $y = -0.15$ m from below the alcove through the center canister and into the ceiling. A vertical dashed line indicates 200°C in each plot. Temperatures far in excess of 200°C would never be considered in an actual design but are included here to illustrate the sensitivity of maximum temperature to the combination of spacing and thermal load.

This corresponds to 40 rooms if the naval fuel is repackaged into approximately 1140 canisters of 1500 W each, or 30 rooms if the naval fuel is repackaged into approximately 1700 canisters of 1000 W each. Thus, by using thermal modeling in conjunction with assumptions about repackaged waste heat loads, we can make predictions that can be used to optimize the repackaging and disposal plans.

III.D. Monte Carlo Simulations

A Monte Carlo sampling of 100 realizations was conducted in which individual canister heat loads were randomly selected from a histogram of waste canister heat loads based on the DOE waste inventory (Table II). Figure 15 shows the lateral and vertical temperature distribution means and 5% to 95% confidence bounds for the 100 Monte Carlo simulations. These plots show the uncertainty in simulated temperatures if randomly selected DOE waste canisters are placed in a room without regard for their individual heat loads. The mean maximum temperature in the salt (outside the canister) is below 60°C with an uncertainty of approximately ± 5°C at the 90% confidence level. From these results, it is clear that a 0.3-m (1-ft) spacing between canisters is sufficient to keep the DOE waste inventory well below 200°C at all times. Assuming 187 canisters per room in this scenario, the 23 032 canisters of DOE waste would require approximately 124 rooms.

IV. CONCLUSIONS

Based on this set of heat flow simulations, we reach the following conclusions:

1. Analytical modeling suggests that temperature variations within the run-of-mine salt between canisters will be smooth and continuous and that coarse numerical discretization will provide reasonable approximations of temperatures. Finer mesh discretization may be required at material interfaces to resolve temperature gradients at those locations accurately.

2. The depth of run-of-mine salt placed over the waste canisters may have complicating effects on temperatures, with temperature increasing with run-of-mine salt depth near the canisters and decreasing within and near the room ceiling.

3. The rate of temperature change at a canister per unit burial depth decreases from 4.8°C/m to 1.5°C/m within the range of the parameter study here.

4. The rate of temperature change per unit canister heat is approximately constant and positive ($\sim$0.3°C/W).

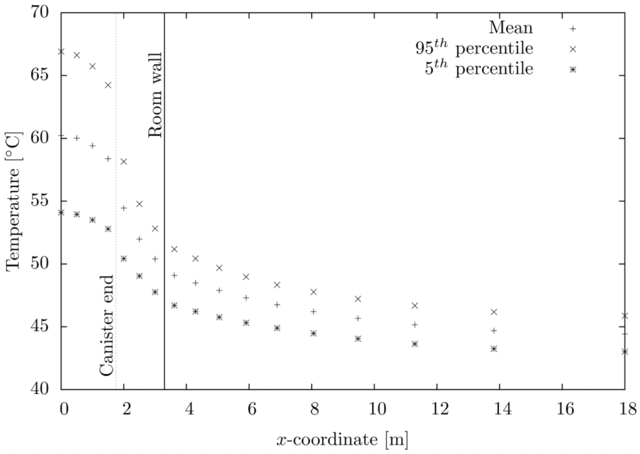

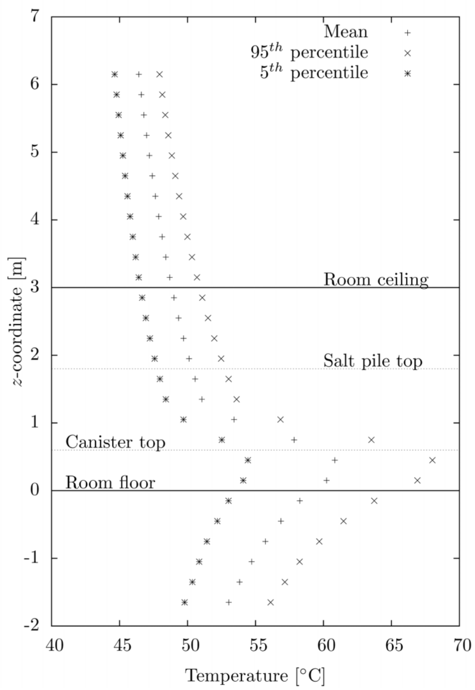

Fig. 15. Simulated steady-state temperatures at finite-volume nodes for various heat loads with centers 0.9 m apart with a 1.8-m depth of run-of-mine salt measured from the floor of the room. Upper plot presents temperature profiles in the x-direction along the line $y = -0.15$ m and $z = 0.15$ m from the center of the room through a canister to the center of the pillar. Lower plot is in the z-direction along the line $x = 0$ m and $y = -0.15$ m from below the room through the center canister and into the ceiling.

5. The rate of temperature change per unit canister spacing decreases from 52°C/m to 24°C/m for DHLW. Maintaining salt temperatures far below 200°C for the DOE waste inventory is feasible, even for closely spaced canisters along the drift.

6. Some SNF waste may have to be repackaged to 1500 or 1000 W per canister with spacings of ~6 and 3 m, respectively, to maintain salt temperatures below 200°C.

7. If DOE waste canisters with randomly selected heat loads are placed in a room, simulations indicate that the maximum salt temperature will be from ~52°C to ~64°C with 90% confidence.

The model simulations presented in this paper are likely an overestimate of the maximum temperatures, since they do not consider either the drop-off of the heat generation curve with time or convective and latent heat effects. As such, they represent a reasonable first approximation of the expected temperature regimes generated by HLW disposed in salt formations for the purpose of evaluating the temperature profiles in a salt repository.

ACKNOWLEDGMENTS

Funding for this work was provided by the Used Fuel Disposition Campaign, Office of Nuclear Energy, of the DOE.

REFERENCES

1. "The Disposal of Radioactive Waste on Land: Report of the Committee on Waste Disposal of the Division of Earth Sciences," Publication 519, National Academy of Sciences/ National Research Council (1957).

2. J. T. CARTER et al., "A Generic Salt Repository for Disposal of Waste from a Spent Nuclear Fuel Recycle Facility," SRNL-RP-2011-00149, Savannah River National Laboratory (2011).

3. F. D. HANSEN and C. D. LEIGH, "Salt Disposal of Heat-Generating Nuclear Waste," SAND2011-0161, Sandia National Laboratories (Jan. 2011).

4. B. A. ROBINSON, N. Z. ELKINS, and J. T. CARTER, "Development of a U.S. Nuclear Waste Repository Research Program in Salt," *Nucl. Technol.*, **180**, 122 (2012); http://dx.doi.org/10.13182/NT11-130.

5. R. A. NELSON and N. BUSCHMAN, "Salt Disposal Investigations to Study Thermally Hot Radioactive Waste in a Deep Geologic Repository in Bedded Salt," presented at Waste Management Conf. 2012, Phoenix, Arizona, February 26–March 1, 2012.

6. E. HARDIN et al., "Generic Repository Design Concepts and Thermal Analysis (FY11)," SAND2011-6202, Sandia National Laboratories (2011).

7. *Final Disposal of High-Level Radioactive Waste in Germany—The Gorleben Repository Project*, Federal Ministry of Economics and Technology (BMWi), Munich, Germany (Oct. 2008).

8. G. A. ZYVOLOSKI et al., "Summary of the Models and Methods for the FEHM Application: A Finite Element

Heat- and Mass-Transfer Code," LA-13307-MS, Los Alamos National Laboratory (1997).

9. "Bibliography of Peer Reviewed Papers Using FEHM for Simulation": fehm.lanl.gov/pdfs/FEHM_references_list.pdf (current as of June 14, 2013).

10. D. J. CLAYTON and C. W. GABLE, "3-D Thermal Analyses of High-Level Waste Emplaced in a Generic Salt Repository," AFCI-WAST-PMO-MI-DV-2009-000002, SAND2009-0633P, LA-UR-09-0089, Advanced Fuel Cycle Initiative (2009).

11. D. E. MUNSON et al., "Overtest for Simulated Defense High-Level Waste (Room B) In Situ Data Report (May 1984–February 1989)," SAND89-2671, Sandia National Laboratories (1989).

12. W. BECHTHOLD et al., "Backfilling and Sealing of Underground Repositories for Radioactive Waste in Salt (Bambus II Project)," Office for Official Publications of the European Communities (2004).

13. H. S. CARSLAW and J. C. JAEGER, *Conduction of Heat in Solids*, 2nd ed., p. 1, Clarendon Press, Oxford, United Kingdom (1959).

14. J. T. CARTER et al., "Fuel Cycle Potential Waste Inventory for Disposition," FCR&D-USED-2010-000031, Rev. 5, U.S. Department of Energy Office of Nuclear Energy (2012).

15. L. LUNDQUIST, "GRIDDER Users Manual," https://meshing.lanl.gov/gridder/users_manual.html (current as of May 1, 2012).

16. B. M. ADAMS et al., "Dakota, A Multilevel Parallel Object-Oriented Framework for Design Optimization, Parameter Estimation, Uncertainty Quantification, and Sensitivity Analysis: Version 5.2 User's Manual," SAND2010-2183, Sandia National Laboratories (2011).